RECENT ADVANCES IN NANOFABRICATION TECHNIQUES AND APPLICATIONS

Edited by **Bo Cui**

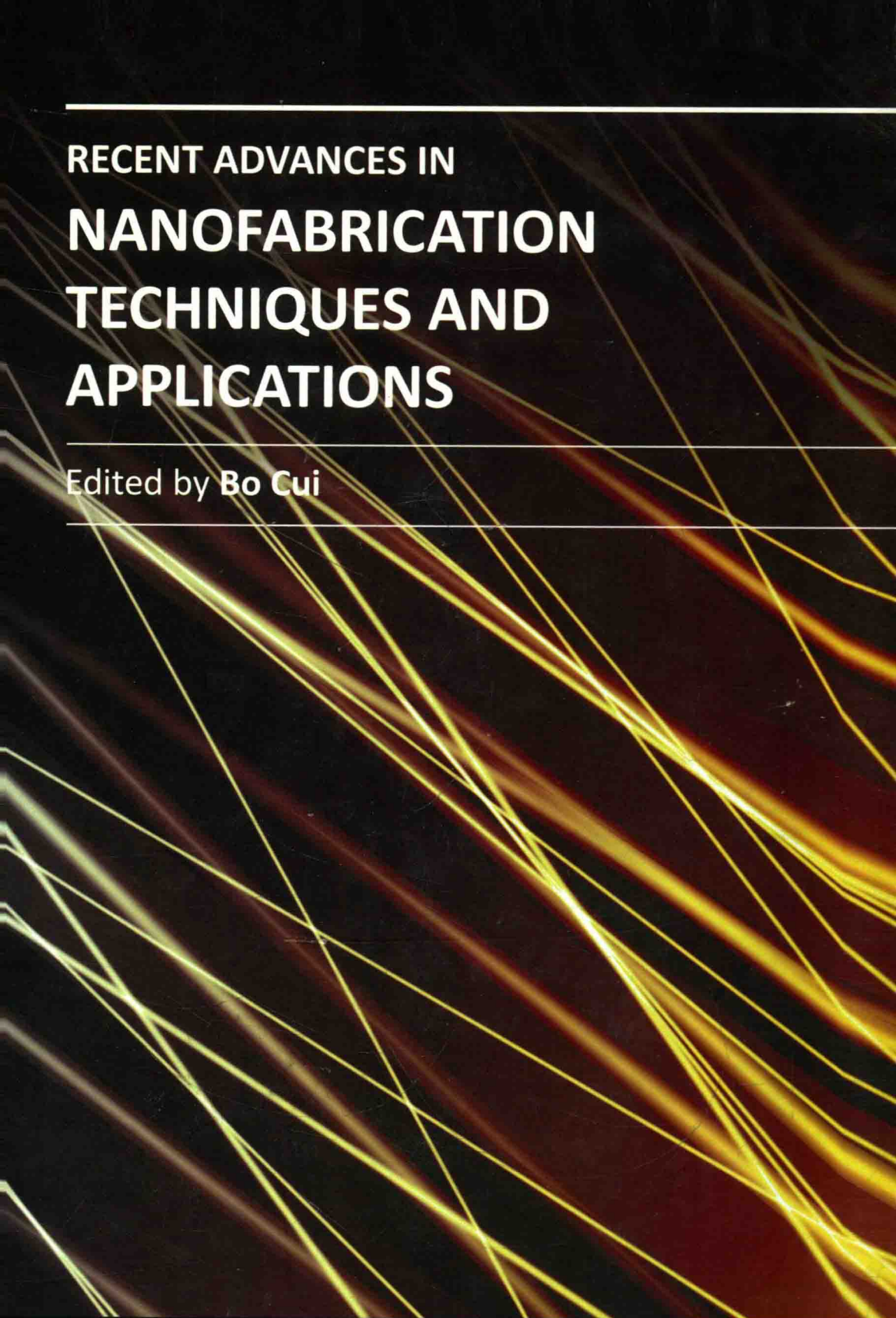

INTECH

RECENT ADVANCES IN NANOFABRICATION TECHNIQUES AND APPLICATIONS

Edited by **Bo Cui**

INTECHWEB.ORG

Recent Advances in Nanofabrication Techniques and Applications
Edited by Bo Cui

Published by InTech
Janeza Trdine 9, 51000 Rijeka, Croatia

Publishing Process Manager Alenka Urbancic
Technical Editor Teodora Smiljanic
Cover Designer InTech Design Team
Image Copyright 2011. Used under license from Shutterstock.com

First published November, 2011
Printed in Croatia

A free online edition of this book is available at www.intechopen.com
Additional hard copies can be obtained from orders@intechweb.org

Recent Advances in Nanofabrication Techniques and Applications, Edited by Bo Cui
p. cm.
978-953-307-602-7

Preface

Nanotechnology has experienced a rapid growth in the past decade, mostly because of the rapid advances in nano-fabrication techniques employed to fabricate the nano-devices. Nano-fabrication can be divided into two categories: the first is the so-called "bottom up" approach, in which nano-structures are created either by chemical synthesis of nano-wires, nanotubes and nano-particles, or by self-assembly of nano-objects or thin layers to form quasi-periodic arrays or phase separation patterns. The second category is the "top down" approach, where nano-structures are created or duplicated from a master mask or mold, using nano-lithography, thin film deposition and etching techniques. Both topics are covered, though with a focus on the second category.

This book aims to provide the fundamentals and the recent advances of nano-fabrication techniques and its device applications. The thirty chapters are a result of contributions from roughly 100 researchers worldwide. Most chapters focus on in-depth studies of a particular research field, and are thus targeted for researchers, though some chapters focus on the basics of lithographic techniques accessible for upper year undergraduate students.

The chapters are divided into five parts. Part I covers lithography based on charged beam, namely electron and focused ion beam lithography, which are the most popular nano-lithographies for R&D. Part II focuses on nano-imprint and soft lithography, which duplicate in parallel a pattern on the mold into a resist layer, and thus have high throughput making them suitable for volume production of nano-devices. Part III contains information on several lithographies using light (UV and X-ray) other than conventional optical lithography. Part IV deals with lithographic techniques relevant only to the next generation integrated circuit fabrication, including extreme UV and deep UV lithography with resolution enhancement techniques. All other lithographic techniques, both bottom up and top down, are grouped in Part V.

In conclusion, I would like to express my sincere gratitude to the contributing authors of each chapter, as well as the publishing process manager, Ms Alenka Urbancic, who spent tremendous time in communicating with me and the authors.

Bo Cui
University of Waterloo
Canada

Contents

Part 1

Electron and Ion Beam Lithography

1

Electron Beam Lithography for Fine Dot Arrays with Nanometer-Sized Dot and Pitch

Sumio Hosaka
Gunma University
Japan

1. Introduction

Recently, electron beam (EB) lithography has been applied to mask and reticle pattern draw, for fabricating semiconductor devices, and nanometer-sized pattern direct writing for developing of new concept nano-device. Mainly, the developing of practical EB drawing system has been started since 1960s, and fine pattern formation has also been studied together with the system development [1-3]. Regarding EB-drawn pattern size, at first, micron and submicron-sized pattern has been drawn on mask blank and directly on the device [4]. Today, the pattern size miniaturizes to nanometer-size of less than 20 nm in research [5, 6].
Especially, I have focused the EB lithography into the possibility to form fine dot and fine pitched dot 2-dimensional arrays for patterned media and quantum devices. The research has been done by dependences of resist material and thickness on drawing of fine dot arrays with nanometer-sized pitch in EB drawing, theoretically and experimentally. I have used Monte Carlo simulation and a conventional EB drawing system combined with scanning electron microscope (SEM) and EB drawing controller [7].
In this chapter, I describe key factors such as resist type, resist thickness, proximity effect, etc for a formation of nanometer-pitch dot arrays, a limitation of the EB-drawn size theoretically and experimentally, and demonstrate the applications to dry-etching process and nano-imprinting.

2. Monte Carlo simulation of electron scattering in solid for EB lithography [8]

Electron scattering in the resist and substrate is described based on its scattering angle, mean free path, energy loss, etc. Trajectories of incident electrons and energy deposition distributions (EDDs) in the resist are calculated. From the EDD, EB drawn resist dot profiles are estimated. The formation of nanometer sized pattern for electron energy, resist thickness and resist type can be studied. The EDD in 100 nm-thick resist on Si substrate were calculated for small pattern drawing. The calculations show that 4 nm-wide pattern will be formed when resist thickness is less than 30 nm. Furthermore, a negative resist is more suitable than positive resist by the estimation of a shape of the EDD.

2.1 Calculation model for Monte Carlo simulation of electron scattering

For the treatment of electron elastic scattering, the screened Rutherford scattering model [11] is employed as follow,

$$\frac{d\sigma_i}{d\Omega} = \frac{e^4 Z_i (Z_i + 1)}{4E^2 (1 - \cos\theta + 2\beta)} \tag{2.1}$$

where the β is the screening parameter which is given by

$$\beta = \frac{1}{4}\left(\frac{1.12\lambda_0 h}{2\pi p}\right), \quad \lambda_0 = Z^{1/3} / 0.885 a_0 \tag{2.2}$$

where the e is electronic charge, th the θ is scattering angle, the a_0 is Bohr radius, the h is Planck's constant and the p is the electron momentum. Step length is calculated based on the electron mean free path Λ. The Λ is given by

$$\Lambda = \frac{1}{n\sigma} = \frac{A}{N\rho\sigma} \tag{2.3}$$

where the n is volume density of atoms, the σ is total cross section calculated from differential scattering cross section, the N is Avogadro's number, the A is atomic weight and the ρ is mass density. Scattering angle θ and azimuthal angle ϕ can be obtained using the following equations:

$$\theta = \cos^{-1}\left(1 - \frac{2\beta R_1}{1 - \beta - R_1}\right), \quad \phi = 2\pi R_2 \tag{2.4}$$

where the R_1 and R_2 are independent equidistributed random number between 0 and 1. Since the electron suffers scattering along its trajectory, it continuously loses its kinetic energy along its trajectory. In Monte Carlo simulation, incident electron is slowing down following Bethe's formula, which is a good empirical method of calculating this energy loss in electron solid interaction. The Bethe's approximation is given by

$$-\frac{dE}{ds} = \frac{2\pi e^4}{E} \sum_i n_i Z_i \ln\left(\frac{1.166E}{J_i}\right) \tag{2.5}$$

where the n_i is volume density of atoms, the J_i is mean ionization energy of atom i . The terminal energy of the nth scattering is:

$$E_{n+1} = E_n - \left|dE / ds\right|_{E_n} \cdot \Lambda_n \tag{2.6}$$

where the E_n is the energy of the (n-1)th scattering, the Λ_n is step length, and the $\left|dE / ds\right|_{E_n}$ is the energy loss rate which can be obtained from Eq. (2.5).

The EDD is an important parameter in consideration of EBL. In order to calculate the EDD in resist, we use cylindrical coordination system. We divide the resist layer along Z-axis into several thin sub-layers. The EDD was calculated in a radius-depth coordination system. This means that the resist layer was devided into many small concentric rings. The simulation was excuted to calculate the total energies $E(r,z)$ in every unit ring for EDD function. The ring volume ΔV is given by following equation,

$$\Delta V = (\pi(r + \Delta r)^2 - \pi r^2) \cdot \Delta Z \tag{2.7}$$

where the ΔZ is the thickness of sub-layer and the Δr is increment in radius direction, From the volume, the EDD function is given by following equation,

$$EDD(r,z) = E(r,z) / (\Delta V \cdot N_0) \tag{2.8}$$

where the N_0 is total number of incident electron.

2.2 Simulation results and discussion

2.2.1 Description and electron trajectories

Monte Carlo simulation has been excuted in energetic electrons impinging in thin film of Si covered with resist material. By using uniform random numbers between 0 and 1, the scattering angles θ and ϕ can be calculated by using Eq. (2.4). Using Eqs. (2.5) and (2.6) ,we can calculate the energy loss ΔE due to scattering of the electrons with atoms in the sample along its trajectory. The trajectory of the electron was traced till its energy slowed down to 50 eV. PMMA $(C_5H_8O_2)$ with a compound of carbon(C), hydrogen(H) and oxygen(O) was used as the typical resist. In the simulation, we use random sampling method to determine the scattering center, the step length and use a new coordinate conversion method [12] for calculating the trajectories of electrons. The initial energies of the incident electrons are taken to be 30 keV and 10 keV. The scattering trajectories of electrons with different incident beam energies in the resist material was used with the same as PMMA resist layer on Si target are shown in Figs. 2. 1- 2. 4. In the simulation, the thickness of the resist layer of 100 nm and the number of incident electrons of 500 was used. With incident energy of 30 keV, the penetration depth was about 3.5μm and lateral range was about 1.5 μm in Si (Fig. 2. 1). In the resist layer, the electron scattering was expanded only to about 20 nm in radius direction (Fig. 2. 2). Although using 10 keV incident electrons can diffuse as deep as 0.5 μm into the sample (Fig. 2. 3) but lateral range was about 50 nm in the resist layer which is larger than that of 30 keV (Fig. 2. 4). It indicated that as the energy decreases, the electrons scattering lateral range is expanded in the thin resist layer at the top.

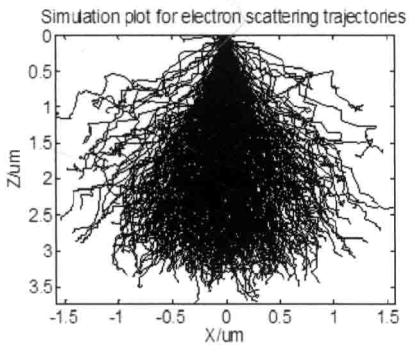

Fig. 2.1. Electron scattering trajectories at incident energy 30 keV

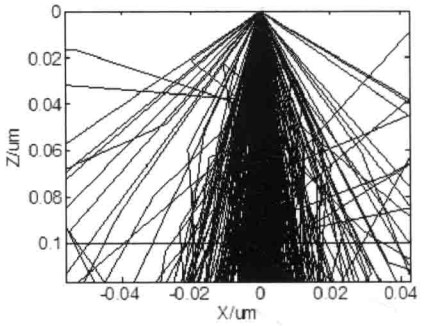

Fig. 2.2. Trajectories in resist (100 nm) at incident energy 30 keV.

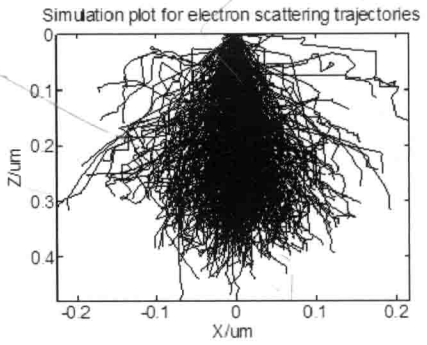

Fig. 2.3. Electron scattering trajectories at incident energy 10 keV.

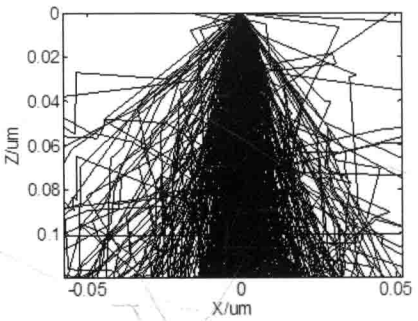

Fig. 2.4. Trajectories in resist (100 nm) at incident energy 10 keV.

2.2.2 Energy deposition distribution (EDD)

The energy deposition density at various positions in depths and radius in the thin resist was calculated. The thickness of the resist was 100 nm, and the incident energy was 30 keV. The ΔZ and Δr were 2nm, and the number of electrons was 30000. Fig. 2. 5 shows the EDD

in the resist layer of various depths 10 nm, 50 nm and 100 nm. It can be clearly seen that the shallower the depth from the surface of the resist, the narrower and the shaper the EDD. Fig. 2.6 shows the relationship between resist depth and standard deviation σ of the EDD assuming that the EDD is approximated by Gauss distribution.

$$EDD(r) = \frac{1}{\sqrt{2\pi}} \cdot \frac{1}{\sigma} \exp\left(-\frac{(r - r_0)^2}{2\sigma^2} \right) \tag{2.9}$$

It indicates that small pattern could be produced by using thin resist. It can effectively reduce proximity effects and thus greatly improve resolution.

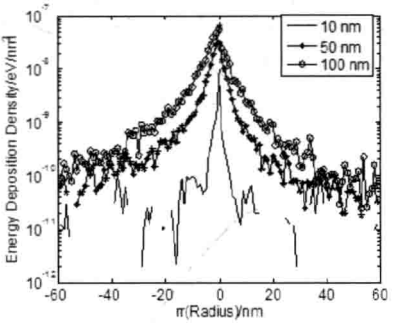

Fig. 2.5. Energy deposition distribution of different depth of resist.

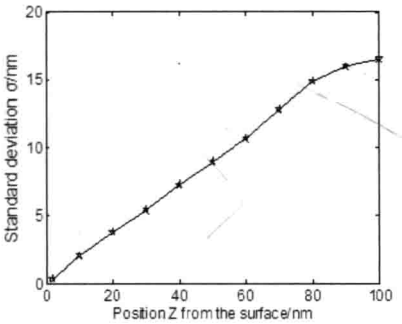

Fig. 2.6. The relationship between resist depth and width of dot.

2.2.3 Consideration for resist development based on EDD

Resist development is assumed as the resist molecule are solved and linked over the critical energy density so that they are soluble and insoluble in positive and negative resists, respectively. Figs. 2. 7(a)-(d) show the area over the critical energy density of 28.125 keV / cm^3 - 0.5 keV / cm^3. It is clear that small pattern formation is possible by selecting large critical energy density, which corresponds to small exposure dosage in experiment. In the positive resist, however, it is very important to solve the top layer at

first. The energy densities of the top layer do not reach to the critical energy density in Figs. 2. 7(a)-(c). As the result, no patterning occurs in the energy region as shown in Figs. 2. 7(e)-(g). When the critical energy density is less than $0.5\,keV/cm^3$, the hole pattern appears as Fig. 2. 7(h). The hole diameter increases with the depth in the resist layer. In our experiment, however, the small diameter of about 4 nm disappears. This may be caused by capillary force. The minimum diameter of about 7 nm was obtained in previous experiment using ZEP520 positive resist [7]. On the other hand, Figs. 2. 7(i)-(l) show the developed resist profiles at various critical energy densities. As the linked molecule is remained on the substrate based on negative resist development mechanism, nanometer-sized patterns are formed as shown in Fig. 2.7(i), although the height of the resist pattern is not complete and short. It is clear that the smaller pattern size is obtained by selecting the heigher critical energy density,but the hight of the resist pattern decreases as the critical energy density increases. Therefore, negative resist is very suitable to form nanometer-sized pattern.

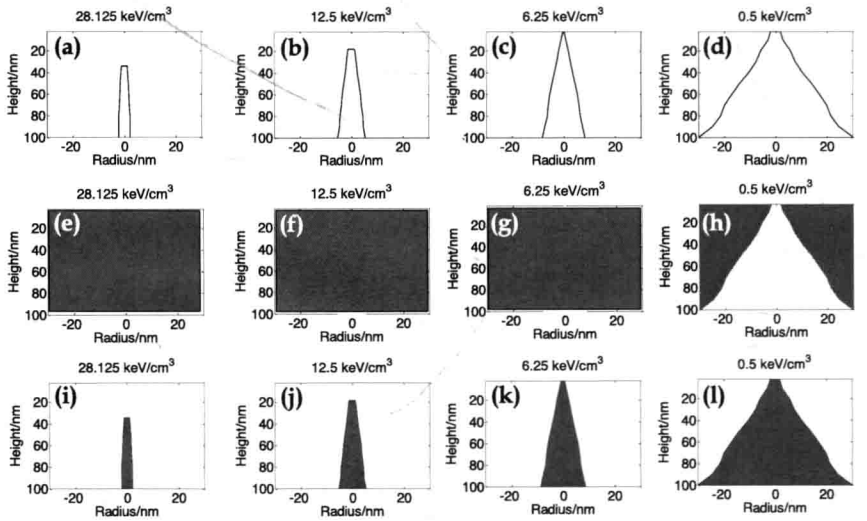

Fig. 2.7. Simulated resist profiles at various critical energies; (a) resist region over 28.125 keV/cm², (b) 12.5 keV/cm², (c) 6.25 keV/cm², (d) 0.5 keV/cm², (e)-(h) positive resist region remained by development, (i)-(l) remained negative resist regions.

3. Formation of highly packed fine pit and dot arrays using EB drawing with positive and negative resists [7, 13]

Fine bit arrays formation for an ultrahigh density optical and magnetic recordings has experimentally been studied using EB drawing with a high resolution scanning electron microscope (HR-SEM), a drawing controller [7] and positive and negative EB resists. As experimental results, calixarene negative EB resist is very suitable to form an ultrahigh packed resist dot arrays pattern, comparing with ZEP520 positive resist as same as described in previous section. We obtained very fine dot arrays with a diameter of <15 nm, and 2-dimensional pitch of <30 nm.